Coenzyme Isomerization Is Integral to Catalysis in Aldehyde Dehydrogenase[†,‡]

Samantha J. Perez-Miller[§] and Thomas D. Hurley*[,||]

Program in Medical Biophysics and Department of Biochemistry and Molecular Biology, Indiana University School of Medicine, Indianapolis, Indiana 46202

Received February 3, 2003; Revised Manuscript Received April 17, 2003

ABSTRACT: Crystal structures of many enzymes in the aldehyde dehydrogenase superfamily determined in the presence of bound $NAD(P)^+$ have exhibited conformational flexibility for the nicotinamide half of the cofactor. This has been hypothesized to be important in catalysis because one conformation would block the second half of the reaction, but no firm evidence has been put forth which shows whether the oxidized and reduced cofactors preferentially occupy the two observed conformations. We present here two structures of the wild type and two structures of a Cys302Ser mutant of human mitochondrial aldehyde dehydrogenase in binary complexes with NAD^+ and NADH. These structures, including the Cys302Ser mutant in complex with NAD^+ at 1.4 Å resolution and the wild-type enzyme in complex with NADH at 1.9 Å resolution, provide strong evidence that bound NAD^+ prefers an extended conformation ideal for hydride transfer and bound NADH prefers a contracted conformation ideal for acyl−enzyme hydrolysis. Unique interactions between the cofactor and the Rossmann fold make isomerization possible while allowing the remainder of the active site complex to remain intact. In addition, these structures clarify the role of magnesium in activating the human class 2 enzyme. Our data suggest that the presence of magnesium may lead to selection of particular conformations and speed isomerization of the reduced cofactor following hydride transfer.

One of the enigmatic features of most crystal structures of aldehyde dehydrogenases with bound $NAD(P)^+$ is the apparent mobility of the nicotinamide half of the cofactor (*1*, *2*). This is seen as missing or weak electron density for the nicotinamide ring and ribose and consequently high temperature factors compared with surrounding protein residues (*3*−*6*). Both the sheep liver cytosolic (ALDH1)[1] and the human liver mitochondrial (ALDH2) aldehyde dehydrogenase structures show density for two distinct conformations, one with the nicotinamide ring in position for hydride transfer (∼3.5 Å from the active site cysteine) and the other with the ring positioned out of the active site by rotations about the pyrophosphate bonds ("hydrolysis" conformation) (Figure 1) (*2*, *7*, *8*). In the initial beef ALDH2 structure with 2 mM Sm^{3+}, the NAD(H) molecules are in the "hydride transfer" conformation with high occupancy, though the nicotinamide half was found to be disordered with 0.2 mM Mg^{2+} (*1*). The adenine half of the cofactor is well-ordered in each structure. The unique interaction of the cofactor with the dinucleotide fold in ALDHs may facilitate a change in the position of the nicotinamide mononucleotide half (NMN) (*1*). Recent NMR studies support the crystallographic observations and indicate that both NAD^+ and NADH exhibit conformational flexibility when bound to human ALDH1 and ALDH2, with NAD^+ showing the greatest mobility (*9*).

The currently accepted model for human ALDH2 catalysis is an irreversible ordered sequential mechanism in which NAD^+ binds prior to aldehyde (*10*). The aldehyde then undergoes nucleophilic attack by Cys302, forming a covalent intermediate (*10*, *11*). Next, the carbonyl hydride is transferred to the A-side of the nicotinamide ring (*9*, *12*). In the rate-limiting step, Glu268 activates a water molecule for nucleophilic attack at the acyl−sulfur bond, releasing the acid product prior to NADH dissociation (*10*, *13*). A suitable water molecule for deacylation is only observed in apo structures and in holo structures with the cofactor in the hydrolysis position (*1*, *8*) (Figure 1). Thus, it has been hypothesized that isomerization is integral to catalysis: the reduced nicotinamide ring must be displaced for the deacylating water to be properly positioned and activated by Glu268 for completion of the reaction. We present here four previously unpublished structures of human ALDH2 in complex with both the oxidized and reduced coenzyme which provide insight into the importance of cofactor isomerization in catalysis. In addition, human ALDH2 is activated 2-fold by magnesium at physiological levels, though this does not appear to result from an increase in the number of functioning active sites (*14*, *15*, *16*). Comparison with structures in the presence of a low level of magnesium suggests a mechanism whereby the addition of metal ion could speed the reaction.

[†] This work has been supported by NIH Grant AA11982.

[‡] Coordinates and structure factors have been deposited with the Protein Data Bank. The PDB codes are listed in Table 1 and in the Supporting Information.

* To whom correspondence should be addressed: Department of Biochemistry and Molecular Biology, Indiana University School of Medicine, Indianapolis, IN 46202. Phone: (317) 278-2008. Fax: (317) 274-4686. E-mail: thurley@iupui.edu.

[§] Program in Medical Biophysics.

[||] Department of Biochemistry and Molecular Biology.

[1] Abbreviations: NAD, nicotinamide adenine dinucleotide; ALDH1, liver cytosolic aldehyde dehydrogenase; ALDH2, liver mitochondrial aldehyde dehydrogenase; AMP, adenosine monophosphate; NMN, nicotinamide mononucleotide.

10.1021/bi034182w CCC: $25.00
Published on Web 05/20/2003

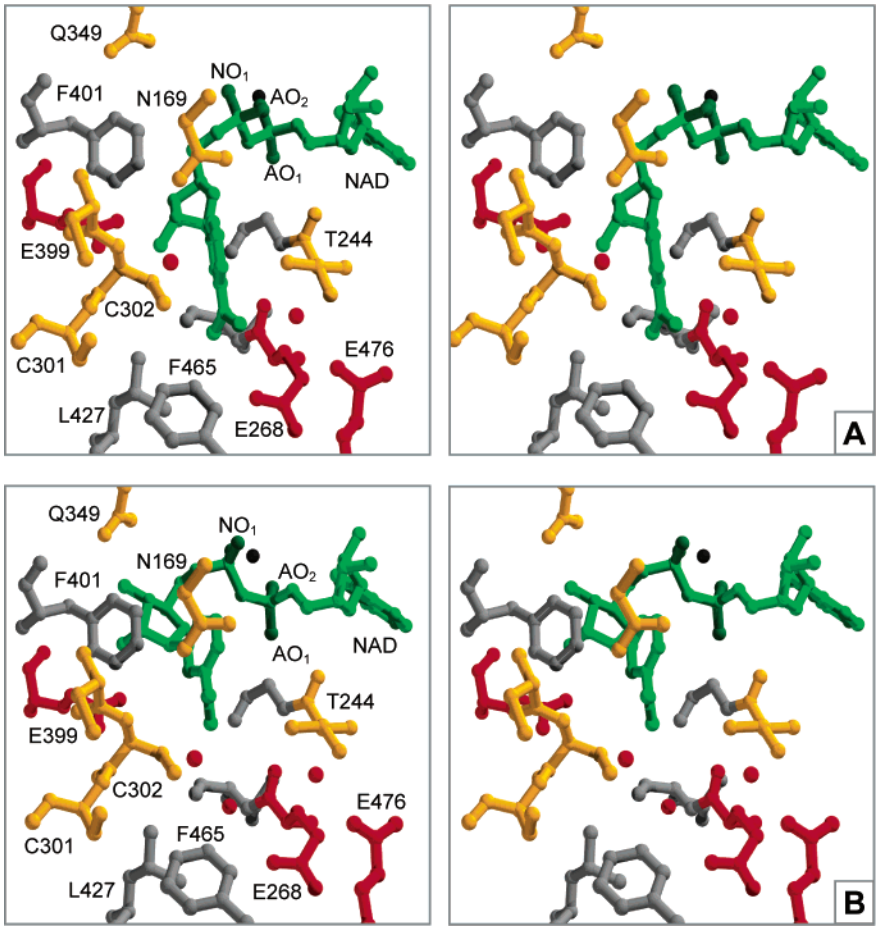

FIGURE 1: Stereodiagrams of active site configurations seen in human ALDH2 [PDB entry 1CW3 (*7*)]. (A) Hydride transfer conformation seen in three active sites. (B) Hydrolysis conformation seen in five active sites. The phosphate oxygens of NAD(H) are shown in dark green. NO_1 and AO_2, which interact with the Mn^{2+} (black sphere), are pointing back from this view. For clarity, Asn169 is shown without the backbone atoms.

EXPERIMENTAL PROCEDURES

Materials. NADH, DTT, DEAE-Sepharose, *p*-hydroxyacetophenone, guanidine-HCl, glycerol, and ethylene glycol were purchased from Sigma Chemical Co. (St. Louis, MO). ACES buffer, $MgCl_2$, propionaldehyde, and crotonaldehyde were from Aldrich Chemical Co., Inc. (Milwaukee, WI). Grade I NAD^+ was from Roche Diagnostics Corp. (Indianapolis, IN). Bio-Rad protein assay reagent was from Bio-Rad Laboratories (Hercules, CA). Polyethylene glycol (PEG) 6000 MW was from Hampton Research (Laguna Niguel, CA).

Oligonucleotide-Directed Mutagenesis. Wild-type cDNA for human ALDH2 cloned into the pT7-7 plasmid was obtained from H. Weiner at Purdue University (West Lafayette, IN) (*17*, *18*). PCR-based site-directed mutagenesis was completed with the Stratagene (La Jolla, CA) QuikChange kit using oligonucleotides obtained from Gibco BRL (Life Technologies, Grand Island, NY). Mutations were confirmed by DNA sequencing. Plasmid purification was performed using the Qiagen (Valencia, CA) Midi and Maxi Plasmid purification kits, using a protocol slightly modified from the manufacturer's instructions to increase yields.

Protein Expression and Purification. Procedures for expression and purification of ALDH2 have been published (*18*−*20*). Briefly, wild-type and mutant cDNAs were expressed in *Escherichia coli* BL21(DE3) cells, and enzymes were purified using DEAE-Sepharose and *p*-hydroxyacetophenone affinity chromatography. Protein was dialyzed and then concentrated in an Amicon stirred cell (Millipore Corp., Bedford, MA) before being stored at −20 °C in a solution containing 50% glycerol. To prepare for crystallization trials, protein was dialyzed exhaustively into three changes of 10 mM ACES buffer at pH 6.6 with 1 mM DTT and then concentrated to 6−8 mg/mL in an Amicon Centricon YM30. The protein concentration was monitored using the Bio-Rad protein assay with bovine serum albumin as the standard. Activity was monitored by following NADH production by absorption at 340 nm and 25 °C with a Beckman DU 640 spectrometer. Standard activity assays were conducted in 100 mM sodium phosphate buffer at pH 7.5, with 1.5 mM NAD^+, and propionaldehyde at 200 μM for the wild type or 8 mM for the Cys302Ser mutant.

Crystallization. All crystallization trials were set up using the sitting drop geometry in a reduced oxygen environment to limit oxidation of a surface cysteine. Trays were then incubated at 20 °C for 3−6 weeks. Crystallization solutions normally consist of 100 mM Na-ACES (pH 6.2−6.6), 15−19% (w/v) PEG 6000 MW, 100 mM guanidine-HCl, 10 mM $MgCl_2$, and 8 mM DTT. Starting protein concentrations were 8 mg/mL for the wild type and 6.5 mg/mL for the Cys302Ser mutant.

Data Collection and Refinement. Home source X-ray data have been collected with the Rigaku RU200HB X-ray

generator and either a RAXIS IIC or IV^{++} image plate detector. Crystals were soaked in a crystallization solution with added NAD$^+$/H, cryoprotected with 18−22% ethylene glycol, and then flash-cooled in an N_2 gas stream at −165 °C, or more recently at −180 °C. Synchrotron data were collected at the Advanced Photon Source (APS) at Argonne National Laboratory (Argonne, IL) on beamline SBC-CAT 19ID and at the National Synchrotron Light Source (NSLS) at Brookhaven National Laboratory (Upton, NY) on beamlines X12B and X12C. The APS data were indexed, integrated, and scaled with the HKL2000 Program Suite. NSLS and home source data collection and processing were conducted using the programs Strategy and HKL (*21*). Cross-validated data sets were created using the CCP4 suite (*22*). Unless otherwise noted, models were refined using the Crystallography and NMR System (CNS) (*23*) and manually rebuilt using O (*24*). Molecular figures were created with Swiss PDB Viewer (*25*) and POV-Ray (*26*). In most cases, the protein coordinates from a preceding model were used directly for rigid body refinement, as the cell parameters vary only slightly from crystal to crystal within the same space group. Following initial maximum likelihood positional and *B*-factor refinement, the heteroatom free, sigma-A-weighted $2F_o - F_c$ and $F_o - F_c$ maps were inspected, and the appropriate cofactor conformation was built into each subunit. To reduce model bias, the models were then subjected to one round of simulated annealing prior to automated water picking and further refinement and rebuilding.

RESULTS

Each of the structures presented here was determined from the orthorhombic space group and has two tetramers in the asymmetric unit. Root-mean-square deviations (rmsds) for backbone atoms between tetramers are all less than the estimated coordinate errors (<0.3 Å). Noncrystallographic symmetry rmsds within each tetramer are all less than 0.15 Å, showing no asymmetry among the subunits that might explain half-site reactivity. The data collection and refinement statistics are listed in Table 1, and information about three additional structures has been provided as Supporting Information.

Wild-Type ALDH2 with Rapid NAD$^+$ Soak. A 2.6 Å data set was collected on a crystal grown in the apo form and soaked for 6 min in the crystallization solution containing 2 mM NAD$^+$ (pH 6.4). The structure was determined and refined starting with apo-ALDH2 coordinates [PDB entry 1o05 (*8*)] for initial rigid body fitting and refined using CNS, including an anisotropic bulk solvent correction and individual restrained isotropic temperature factors for all atoms. For positional minimization, moderate NCS restraints were used on backbone atoms for residues 15−500, as density for the first six residues is not usually observed, and residues 7−15 vary in position between monomers.

Initial maps showed clear difference electron density for both conformations of the cofactor; thus, refinement rounds were done in parallel, with both the hydride transfer and hydrolysis conformations at full occupancy, with no discernible difference in protein conformation between the two (Figure 2). The final round of refinement included both conformations, each at 50% occupancy based on peak heights

Table 1: Data Collection and Refinement Statistics[a]

	wild type	wild type	Ser302	Ser302
coenzyme	NAD$^+$	NADH	NAD$^+$	NADH
soak time (min)	6	30	15	105
[Mg^{2+}] (mM)	10	10	10	10
PDB entry	1o00	1o02	1o04	1nzw
resolution (Å)	30−2.60	25−1.90	50−1.42	25−2.65
total no. of observations	271631	1379118	3220059	369577
no. of unique observations	111139	291666	683580	100497
completeness (%)[b]	94.4 (81.6)	98.6 (90.4)	95.8 (74.0)	91.8 (72.4)
$\langle I/\sigma I \rangle$	14.6 (5.1)	19.2 (2.8)	20.7 (1.8)	8.1 (2.4)
R_{merge} (%)	4.6 (12.6)	6.7 (35)	6.0 (43.9)	11.4 (40.2)
R_{work} (%)	19.3	18.1	14.5	21.8
R_{free} (%)[c]	23.2	21.4	17.1	25.2
rmsd for bonds (Å)	0.006	0.008	0.014	0.006
rmsd for angles (deg)	1.41	1.46	1.50	1.26
NCS rmsd	0.07	0.10	0.12	0.06
overall *B*-factor	16.9	22.3	12.8	28.4
no. of waters	1772	3584	5025	820
nicotinamide position	both	hydrolysis	hydride transfer	hydrolysis

[a] Space group $P2_12_12_1$. Cell dimensions: $a = 141 \pm 1$ Å, $b = 152 \pm 1$ Å, and $c = 177 \pm 0.5$ Å. [b] Values for the highest-resolution shell are shown in parentheses. [c] R_{free} was determined from a randomly selected 5% of the reflections.

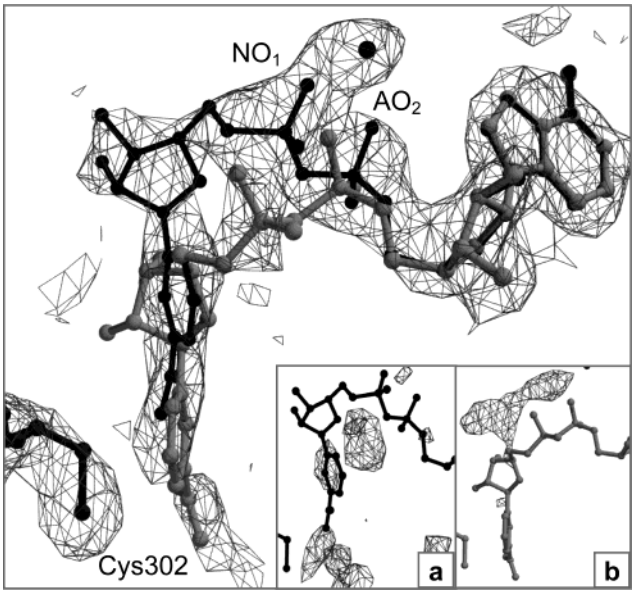

FIGURE 2: Cofactor conformations observed in the wild-type, NAD$^+$ structure. The hydride transfer conformation is shown in gray; the hydrolysis conformation is shown in black, and the Mg^{2+} is also shown in black. (a) Difference map resulting from modeling the cofactor in only the hydrolysis conformation. (b) Difference map resulting from modeling the cofactor in only the hydride transfer conformation. Maps are contoured at 1σ for $2F_o - F_c$ and at 2.8σ for $F_o - F_c$ (insets).

in the difference maps. The average *B*-factor distributions for the cofactors show a sharp increase over the phosphodiester linkage (Table 2). A single magnesium ion is modeled near the adenosine and nicotinamide phosphate oxygens, AO_2 and NO_1 (Figures 1 and 2), in a position assumed to be the average for both cofactor conformations. The hydration sphere surrounding the Mg^{2+} is not discernible in the electron density maps.

Wild-Type ALDH2 and NADH. Data were collected at beamline X12B at NSLS to 1.9 Å on a crystal grown in the apo form and soaked for 30 min in a crystallization solution

Table 2: Average *B*-Factors (Å^2) for AMP and NMN of the Cofactor[a]

structure	adenine through AC_5*	NC_5* through nicotinamide	difference
wild-type NAD^+	18.4[b]	31.9[b]	13.4[b]
wild-type NADH	20.3	22.9	2.6
Ser302 NAD^+	13.1	16.1	3.0
Ser302 NADH	23.8	25.1	1.2

[a] Average values determined over eight cofactor molecules. [b] Average over the two conformations.

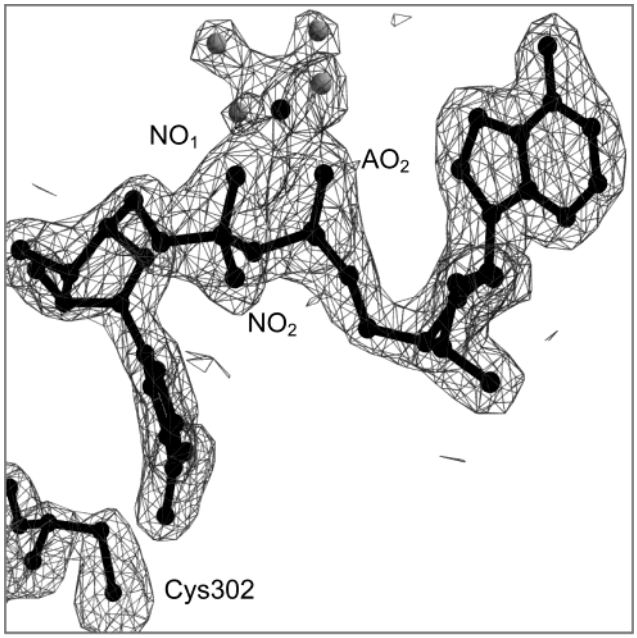

FIGURE 3: Hydrolysis conformation observed in the wild-type, NADH structure. The Mg^{2+} is shown in black with the surrounding water in gray. The $2F_o - F_c$ map is contoured at 1σ. To highlight the metal ion interactions, this view differs slightly from that in Figures 2 and 4.

containing 0.6 mM NADH (pH 7.0). This structure was determined using the apo-ALDH2 protein coordinates (*8*) for initial rigid body fitting and refined using CNS and O in the same manner indicated above for the wild-type NAD^+ complex. The density clearly shows all of the cofactors in the hydrolysis conformation. The average *B*-factor distribution for the NADH shows only a minor increase from the adenine to the nicotinamide end (Table 2). The Mg^{2+} is bound to AO_2 and NO_1, at average distances of 2.1 Å. The water structure is clearly visible, with each subunit showing density for four molecules of solvent that complete an octahedral arrangement around the metal ion (Figure 3). Though there is no direct contact between the magnesium ion and the protein, water molecules in the hydration shell do make contacts with Ser246 directly and with Glu195 and Gln196 through second and third hydration shells.

Although visual inspection of the maps suggests that a puckered nicotinamide ring may make a better fit to the density, the resolution of this data set does not warrant the release of planar restraints on the ring, and thus, we have retained a planar nicotinamide in the model.

Cys302Ser ALDH2 and NAD$^+$. Data were collected to 1.42 Å at beamline 19ID at APS on a Cys302Ser mutant crystal grown in the apo form and then soaked in a crystallization solution containing 2 mM NAD^+ for 15 min (pH 6.4). This

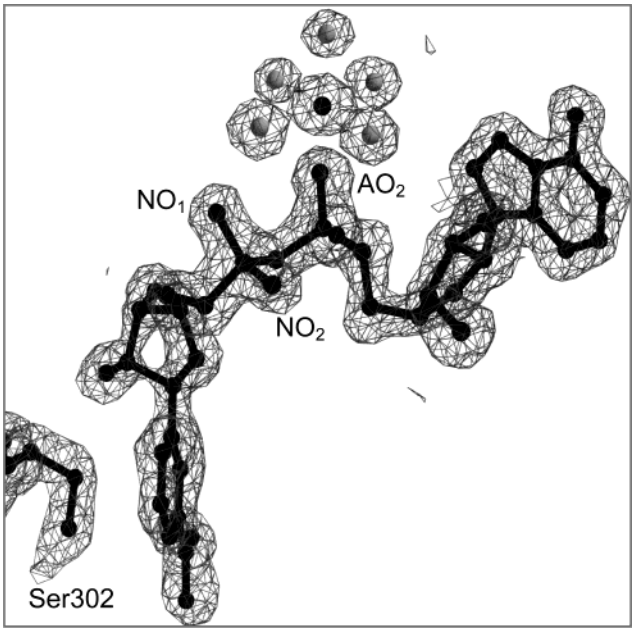

FIGURE 4: Hydride transfer conformation observed in the Ser302, NAD^+ structure. The Mg^{2+} is shown in black with the surrounding water in gray. The $2F_o - F_c$ map is contoured at 1σ.

structure was determined using the apo-ALDH2 coordinates (*8*), as described above, and refined without NCS restraints using CNS, REFMAC5 (*27*), and O. All eight bound cofactors are observed to be in the hydride transfer conformation. A final rmsd for C_α atoms in a tetramer when compared to the wild-type structure is 0.2 Å, indicating that there has been little perturbation of the tertiary structure due to the mutation. The average coenzyme *B*-factor distribution shows only a small increase from the adenine to the nicotinamide end (Table 2). The Mg^{2+} is coordinated directly to AO_2 at an average distance of 2.1 Å, with five water molecules completing the octahedral arrangement, one of which bridges the increased distance to NO_1 (Figure 4). The contact of water molecules in the hydration shell differs from the NADH structure in that the direct contact with Ser246 no longer occurs; instead, a second water sits between the residue and the hydration shell. In addition, water molecules in the primary hydration shell now make contact with Glu195 and Gln196.

The resolution of this structure has permitted us to assign a second metal site to Na^+, previously modeled as a water molecule. This site has a distorted octahedral coordination with only oxygen atoms at an average distance of 2.6 Å, consistent with that expected for a sodium (*28*). That it is not a magnesium site is further supported by the observation of the metal site even in those structures in which the crystal was grown without Mg^{2+} or had a 50-fold reduction in the Mg^{2+} concentration. The Na^+ site may be structurally important for anchoring the loop containing Lys192 and Glu195 which form critical contacts with the cofactor (Figure 5). The role of monovalent ions in the structure and activity of ALDHs has not been investigated.

Cys302Ser ALDH2 and NADH. A 2.65 Å data set was collected on a Cys302Ser mutant crystal grown in the apo form and then soaked in a crystallization solution with NADH in two steps: 45 min at 0.5 mM NADH (pH 6.8) and 60 min at 1 mM NADH (pH 7.0). The structure was determined starting with the protein coordinates from the

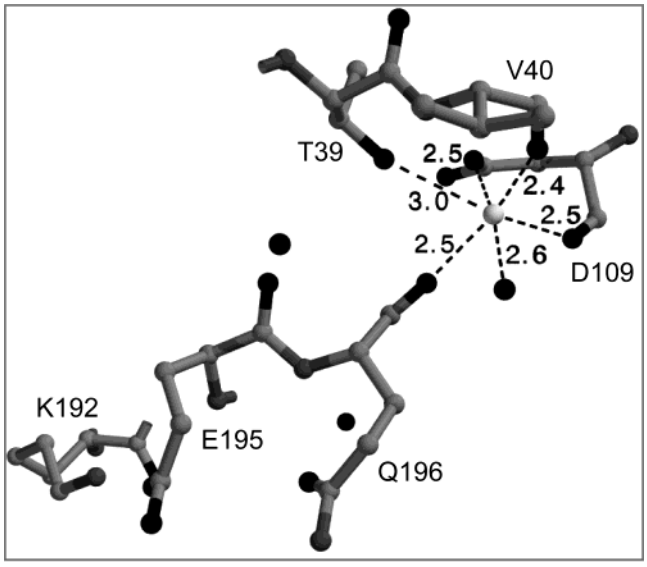

FIGURE 5: Location of the sodium site in the Ser302, NAD^+ structure. Sodium is shown in light gray with average distances to nearby oxygen atoms (shown in black). Nitrogen atoms are shown in dark gray and carbons in light gray.

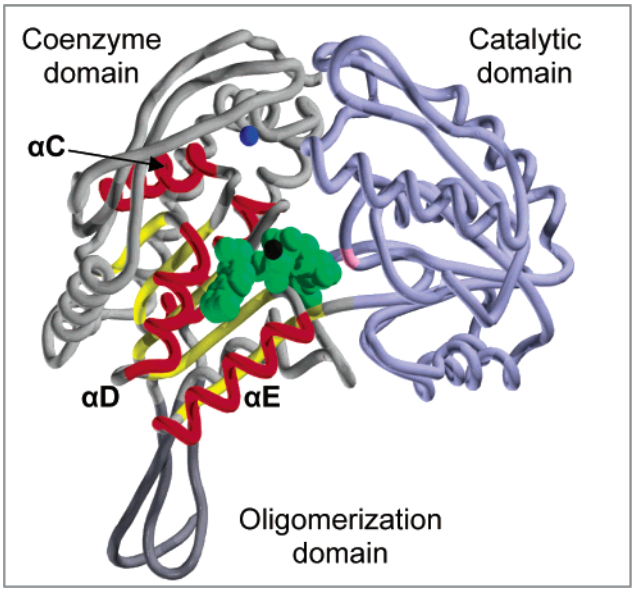

FIGURE 6: ALDH2 monomer with the dinucleotide binding domain highlighted in red helices and yellow strands. NAD^+ is shown in light green, Mg^{2+} in black, Na^+ in blue, and the location of Cys302 in pink.

Cys302Ser−NAD^+ complex for initial rigid body fitting and refined using CNS and O as indicated above for the wild-type NAD^+ complex. The cofactors are all in the hydrolysis conformation with an average *B*-factor distribution similar to that of the wild type with NADH. The Mg^{2+} is within 2.2 Å of AO_2 and NO_1, but the surrounding water structure is not defined in the maps.

DISCUSSION

As the structure of ALDH2 has been discussed in detail (*1*), this description will be limited to the specific contacts made by the two observed conformations of the cofactor. Both conformations have in common the contacts surrounding the adenosine monophosphate portion (AMP) of NAD(H). The adenine ring binds at the surface of the enzyme in a hydrophobic pocket formed by helices αD and αE of the dinucleotide binding fold (Figure 6). The adenine ribose oxygens are within hydrogen bonding distance of the side chains of Lys192, Glu195, and the backbone oxygen of Ile166. The surface-exposed pyrophosphate bridge is partially stabilized by the off axis helix dipole of helix αE, potential hydrogen bonds with the side chains of Ser246 and Trp168, and coordination to a magnesium ion.

In the hydride transfer conformation, AO_2 is directly coordinated to the metal ion while a water molecule bridges the gap between the Mg^{2+} and NO_1 (Figure 7A). NO_1 and NO_2 are within hydrogen bonding distance of Nϵ1 of Trp168. The nicotinamide ribose oxygens are within hydrogen bonding distance of the side chain of Glu399, and the ring is flanked by the backbone of Gly245 and the Phe401 ring at ∼3.5 Å on either side (Figure 8A). The nicotinamide ring is sandwiched between the side chain of Cys302 and Cγ2 of Thr244, each ∼3.4 Å from the ring. The NH_2 of the carboxamide group is within 3 Å of the carbonyl oxygen of Leu269.

In the hydrolysis conformation, both AO_2 and NO_1 are directly coordinated to the metal and only NO_2 is within hydrogen bonding distance of Nϵ1 of Trp168 (Figure 7B). The nicotinamide ribose is shifted by ∼3.5 Å toward the surface and rotated nearly 80°. The ribose oxygens are within hydrogen bonding distance of the side chains of Glu399 and Gln349, and the faces of the ring no longer have close contacts. The nicotinamide ring, shifted by ∼4 Å and rotated by ∼30°, approximately occupies the former position of the ribose, sandwiched between the backbone of Gly245 and the side chain of Phe401 (Figure 8B). The carboxamide NH_2 is within hydrogen bonding distance of the carbonyl oxygens of Leu269 and Glu245, and the carboxamide oxygen is within 3 Å of the amide nitrogen of Asn169.

In summary, there are small shifts in the potential hydrogen bonding network, a loss of close packing contacts for the ribose ring, and the exchange of a polar (Cys or Ser302) for a hydrophobic contact (Phe401) for the nicotinamide ring. The latter difference suggests that the hydrolysis conformation may be favorable for NADH and the hydride transfer conformation for NAD^+.

Isomerization of the bound cofactor is made possible by a mode of interaction with the dinucleotide fold in ALDHs that is distinct from other $NAD(P)^+$-dependent enzymes. In effect, the AMP has "slipped" down helix αE of the Rossmann fold so that the adenine ring rests in a cleft between helices αD and αE. The result is that the phosphodiester bridge, now pointing away from the protein, is solvent-exposed (Figure 9). The metal ion coordination and the absence of a strong helix dipole interaction permit the phosphates to orient in multiple positions while the cofactor is bound. In contrast, in alcohol dehydrogenase (ADH), representative of canonical dinucleotide binding (*28*, *29*, *31*), the phosphates point toward and are almost entirely buried in the interface between the catalytic and coenzyme binding domains (*32*, *33*). Rotational isomerization of the phosphates is severely restricted due to domain closure after cofactor binding and the resultant tight hydrogen bonding network that fixes the residues that interact with the phosphate oxygens (*32*, *34*). The difference in binding is also evident in the disparity in the number of contacts made with the

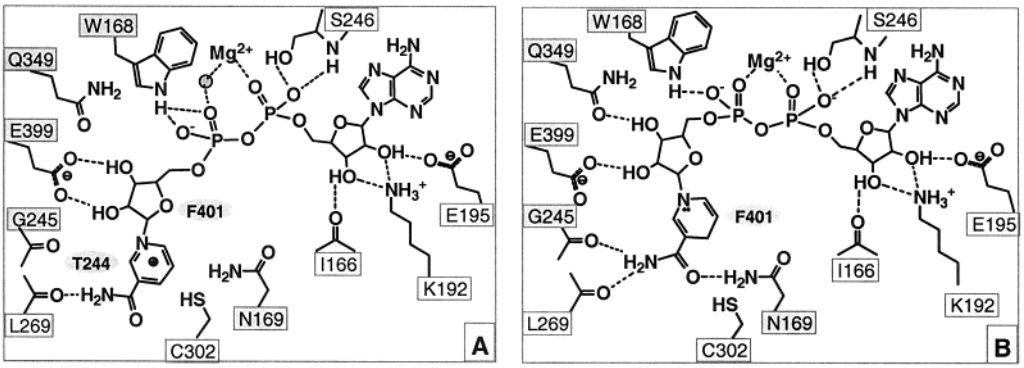

FIGURE 7: Interactions of the cofactor with surrounding residues, based on the four structures presented here. Potential hydrogen bonds are shown with dashed lines for contacts between 2.5 and 3.2 Å in length: (A) hydride transfer conformation and (B) hydrolysis conformation. This figure was created using ChemWindow (Sadtler Division, Bio-Rad Laboratories, Grand Junction, CO).

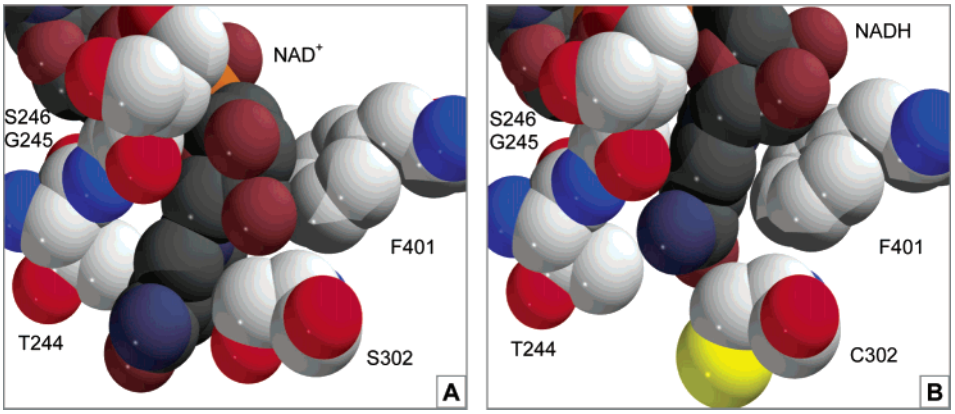

FIGURE 8: Close contacts made by the nicotinamide ribose and ring. Plots of van der Waals surfaces in the active site for the (A) hydride transfer conformation seen in the Ser302, NAD^+ structure and (B) hydrolysis conformation seen in the wild-type, NADH structure.

protein. In ADH, the phosphates have 21 protein contacts within 4 Å, whereas in ALDH2, this number is 13 for the hydride transfer conformation and 8 for the hydrolysis conformation, the rest being supplied by the coordinating metal and solvent. The remainder of the cofactor molecule has approximately the same number of close contacts in both enzymes, except for the adenine ring which appears to interact more closely with the protein in ALDH2, possibly to counterbalance the less constrained binding of the pyrophosphates.

It is hypothesized that isomerization of the coenzyme is a significant and necessary feature of catalysis (*1*, *2*). The ideal placement of the nicotinamide ring for hydride transfer conflicts with the position of the only observed candidate for a deacylating water molecule and would separate Glu268 from the acyl−enzyme intermediate (Figure 10) (*1*, *8*). As deacylation is rate-limiting for ALDH2 and NADH does not dissociate from the enzyme until after this step, it would appear that isomerization to the hydrolysis position is required for completion of the second half of the reaction. From a mechanistic standpoint, it is not essential that NAD^+ bind only in the hydride transfer and NADH only in the hydrolysis position. The coenzyme could, in fact, occupy both conformations as long as the predominant position for each did not interfere with the reaction and the rate constant for isomerization was faster than that for the chemical steps.

The Observed Conformation of NAD^+ but Not NADH Is Dependent on Enzyme Activity. Experiments designed to obtain a highly desirable ternary complex have so far resulted only in binary complexes, with the exception of one low-occupancy, noncovalent complex with crotonaldehyde or its product. Binary complex or ternary complex attempts with the wild-type enzyme and NAD^+ have consistently shown mixed conformations for the cofactor, or more frequently, only the hydrolysis conformation, while all complexes with NADH show only the hydrolysis conformation. These observations suggested that the enzyme was turning over in the crystal. Kinetic experiments confirmed the presence of aldehydes at approximately 0.5 mM in the polyethylene glycol 6000 MW (PEG6K) used as a precipitant for crystallization. The observation of mixed or hydrolysis conformations in soaks with NAD^+ is consistent with reduction to NADH, and these structures likely contained a mixture of NAD^+ and NADH. With this in mind, further binary complex experiments were designed with the goal of limiting or preventing the enzyme from oxidizing the unidentified aldehydes in the crystallization and soak solutions.

In one attempt to limit enzyme turnover, a data set was collected on a binary complex in which the NAD^+ was introduced into the crystal with a soak time of 6 min. The coenzyme is bound with full occupancy, but both nicotinamide conformations are observed and modeled into each subunit (Figure 2). Coenzyme temperature factor distributions for this and other structures of wild-type crystals soaked with NAD^+ show increases of approximately 15 $Å^2$ from the adenine to the nicotinamide end, regardless of the modeled cofactor conformation. As differences in *B*-factors cannot, by themselves, differentiate between static and dynamic disorder, the jumps could be due to an increased mobility of bound NAD^+ over NADH and/or to an averaging of two

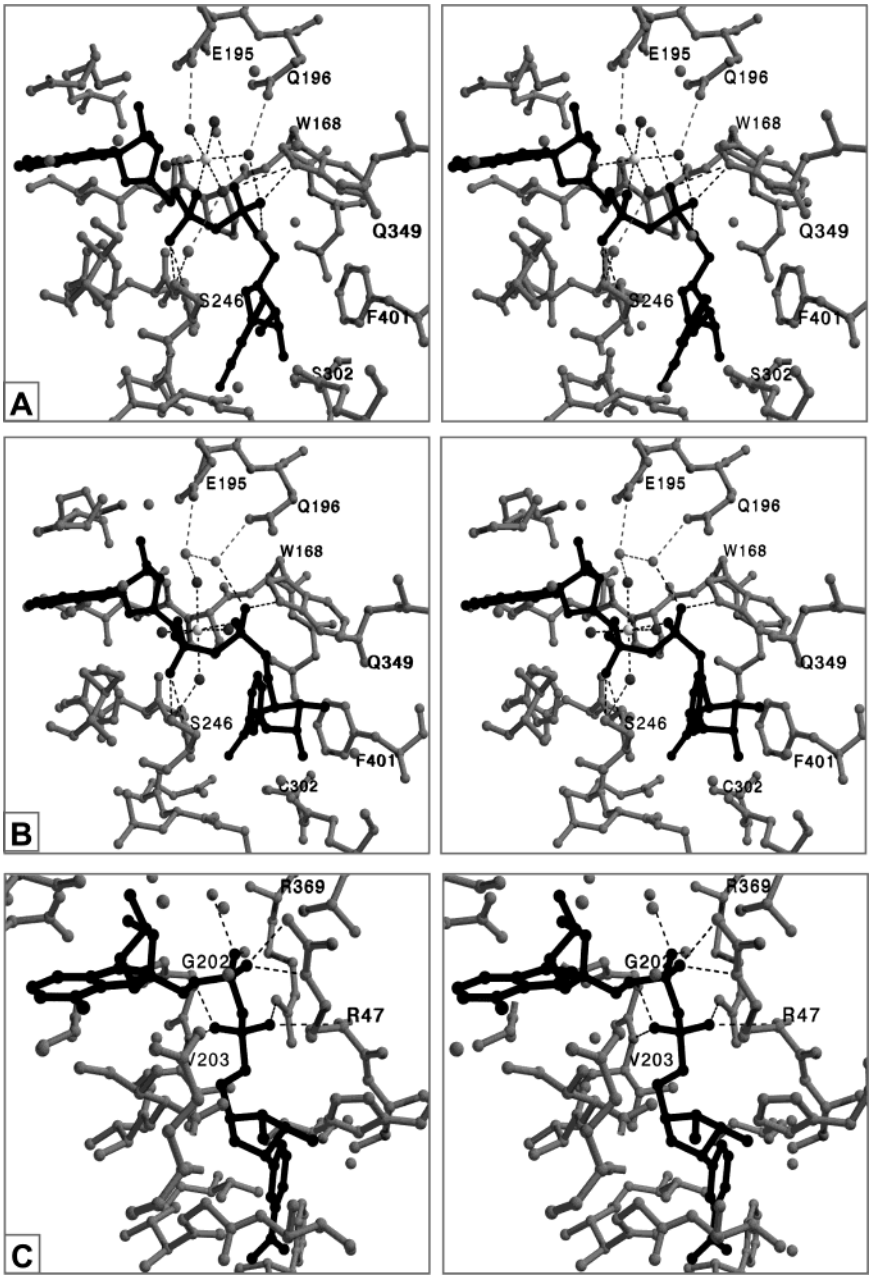

FIGURE 9: Stereoviews of cofactor binding. (A) Hydride transfer conformation seen in the Ser302, NAD^+ structure. (B) Hydrolysis conformation seen in the wild-type, NADH structure. The Mg^{2+} is shown in light gray with first-hydration shell water molecules in dark gray. (C) Cofactor binding in the class 1 alcohol dehydrogenase, ADH1C2 [PDB entry 1HT0 (*33*)]. Potential hydrogen bonding contacts are shown with dashed lines.

or more static conformations. If the oxidized and reduced rings occupy different positions, and the structure contains a mixture of NAD^+ and NADH, as is likely for the wild-type enzyme soaked with NAD^+, then the jump in temperature factors could be interpreted as resulting primarily from static disorder in addition to any motional averaging. On the other hand, if NAD^+ has no conformational preference, the *B*-factor increases would be mostly due to isomerization, even in the case of a mixture of oxidation states. Unfortunately, it is not possible to distinguish between these two possibilities in the case of the wild-type enzyme with NAD^+. However, two structures of a low-activity Ser302 mutant in a binary complex with NAD^+ show all of the cofactors in the hydride transfer conformation. In the 1.4 Å structure presented here, the density for the nicotinamide clearly indicates a planar and thus likely oxidized ring (Figure 4). Interestingly, the coenzyme temperature factor distributions for the Ser302 structures with NAD^+ show only small increases, similar to those observed for NADH. The Ser302 mutant has a specific activity 400-fold lower than that of the wild type at pH 7.5 (S. J. Perez-Miller, unpublished observations), consistent with that observed for the rat mitochondrial enzyme (*11*). The pH of 6.4 used in the crystal soaking experiments would further suppress activity (*13*). Thus, we believe that turnover has not occurred in the Ser302 mutant crystals and that the *B*-factor increases for the coenzyme in these structures are indicative of limited motional averaging of the NAD^+.

As mentioned above, in enzyme complexes with NADH, the hydrolysis conformation has always been observed. The average temperature factor distributions for the NADH in these structures show steady increases of $\sim$3 $Å^2$ from the

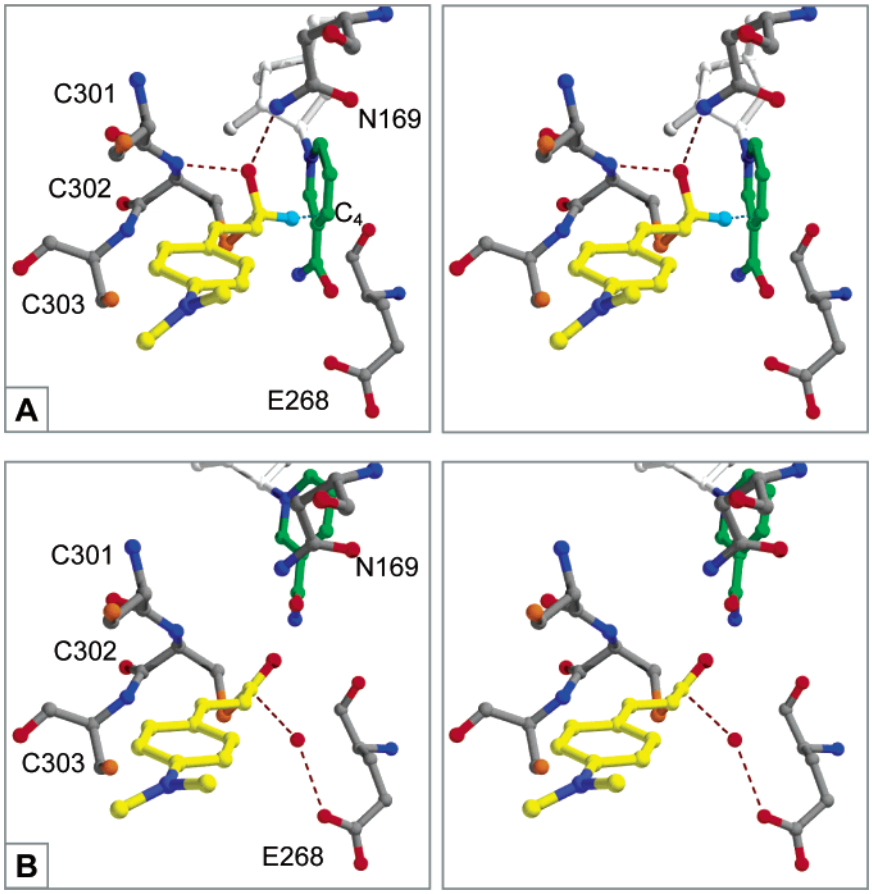

FIGURE 10: Proposed interactions for a thiohemiacetal transition state and an acyl−enzyme intermediate. The substrate (*N*,*N*-dimethylamino)-cinnamaldehyde (DACA) (*36*, *37*) has been used for modeling as the ring structure just fits in the substrate entrance tunnel. Molecules were placed using O, and the positions are consistent with the observed position of binding in a noncovalent complex of ALDH2 (PDB entry 1o01). (A) Hydride transfer conformation of the cofactor with a predicted thiohemiacetal transition state. The oxyanion would be stabilized by the Asn169 side chain and the NH group of Cys302 (*1*), and the hydride (cyan) would be transferred to C4. (B) Hydrolysis conformation of the cofactor with a predicted acyl−enzyme intermediate. In their crystallographically observed positions, Glu268 would activate the indicated water molecule for attack on the modeled Sγ−C bond to release the product. Sulfur atoms are shown in orange, oxygens in red, nitrogens in blue, and carbons in gray for protein atoms, green for the nicotinamide ring, and yellow for DACA. The nicotinamide ribose is shown in white, and the remainder of the molecule has been omitted for clarity. Dashed lines represent interactions of interest less than 3 Å in length.

adenine and ribose rings to the nicotinamide end, indicating that the NMN is not significantly more disordered than the AMP half. At the current maximum resolution of 1.9 Å reported here for the wild-type enzyme, there is no indication of a second conformation in the maps, though motion of the NMN cannot be ruled out (Figure 3). The Ser302 mutant structure with NADH also shows only the hydrolysis conformation, with an even smaller increase in the *B*-factor for the coenzyme (Table 2).

The Absence of Mg^{2+} Results in Increased Disorder for the NMN. Characterization of the human isozymes has shown that ALDH2 is activated and ALDH1 is inhibited by physiological concentrations of Mg^{2+} (*14*, *15*, *16*). The magnesium ion was expected to have the same interactions with the enzyme or cofactor, but elicits opposite effects due to differences in the rate-determining steps of the two enzymes. The addition of Mg^{2+} appears to increase the deacylation rate for ALDH2 and decrease the rate of NADH release for ALDH1 (*15*, *16*). As discussed in Results, a magnesium ion is coordinated to the pyrophosphate group of the cofactor in ALDH2 crystal structures. The binary complexes discussed up to this point were determined in the presence of 10 mM Mg^{2+}. Thus, it is of interest to compare these structures with those determined in the absence of magnesium. A wild-type complex with NAD^+ and approximately 0.2 mM Mg^{2+} shows discontinuous density for the NMN (PDB entry 1nzx). The average *B*-factor distribution for the ADP modeled into this structure is nearly identical to that for the wild-type complex with NAD^+ and 10 mM Mg^{2+}. The loss of interpretable density for the NMN suggests an increase in mobility with a reduced Mg^{2+} concentration. A wild-type structure with NADH and 0.2 mM Mg^{2+} shows the cofactors in the hydrolysis conformation and a loss of higher-contour level electron density for the NMN (PDB entry 1nzz). A 3-fold increase in the cofactor temperature factor distribution jump suggests that the NMN has more mobility than in structures with high Mg^{2+} concentrations. We can then surmise that the Mg^{2+} bound to the pyrophosphate selects and thereby stabilizes the two observed conformations of the coenzyme.

Implications for Catalysis. The picture of catalysis that has emerged from this study provides an important role for nicotinamide isomerization during turnover and suggests that the explanation for metal ion activation lies in the stabilization of particular conformations of the coenzyme. The data suggest that NAD^+ binds predominantly in a conformation

ideal for hydride transfer. Isomerization to the hydrolysis position would occur after hydride transfer to permit deacylation. Because the direct interaction with both AO_2 and NO_1 will be more favorable than the water-mediated interaction seen in the hydride transfer conformation, we suggest that the addition of magnesium ions could accelerate the isomerization step. Without Mg^{2+}, the rate constant for isomerization would be kinetically significant relative to the rate of deacylation. In the presence of Mg^{2+}, the rate of isomerization would exceed that of deacylation, thereby unmasking the true deacylation rate. This could explain how the addition of the magnesium ions increases the enzymatic rate without affecting the number of functioning active sites per tetramer. In contrast, stabilization of NADH by Mg^{2+} may decrease the overall reaction rate in ALDH1, where the release of NADH is rate-limiting (*15*, *16*, *35*).

CONCLUSIONS

The unique mode of cofactor binding to the dinucleotide fold in ALDH permits isomerization of NAD^+ while it is bound to the enzyme, a feat not possible in enzymes that bind $NAD(P)^+$ in the canonical Rossmann manner. Both crystallographic and NMR studies have provided evidence of conformational *flexibility* in a variety of ALDHs, but the question of conformational *preference* has been difficult to tackle. Our data indicate that NADH prefers to occupy the hydrolysis conformation. In fact, we have never observed NADH bound in the hydride transfer position. On the other hand, interpretation of the NAD^+ results is complicated by enzyme turnover in the wild-type enzyme. The argument in favor of conformational preference for the oxidized and reduced cofactor arises from three key observations. The first comes from comparison of the wild-type and low-activity mutant structures. Complexes of the Ser302 mutant with NADH yield only the hydrolysis conformation, and those with NAD^+ show only the hydride transfer conformation. We believe that the latter result is due to the far lower rate of turnover in the mutant crystals. The conformational heterogeneity seen in the wild-type structures can then be explained by oxidation of contaminating aldehydes resulting in various mixtures of NAD^+ and NADH. The second observation comes from comparison of *B*-factor distributions for the various complexes. The contrast between the *B*-factor distributions for NAD^+ and those for NADH supports limited motional averaging in the case where enzyme turnover is prevented or drastically reduced. The third factor comes from the effect of reduced magnesium ion concentrations on the structures. Reduction of magnesium ion concentrations in the binary complexes of the wild-type enzyme results in an increase in disorder for NAD^+ and in a *B*-factor jump for NADH. We argue that these effects are due to increased motional averaging in the absence of Mg^{2+}.

A possible explanation for the observed conformational preferences can be inferred from examining the residues that come into contact with the nicotinamide ring in the two positions. A charged nicotinamide ring in the hydrolysis conformation would be in the proximity of the Phe401 side chain. In the hydride transfer position, the ring comes within 3.4 Å of Cys302 at Cβ and Sγ. As Sγ is, at the very least, polar and is expected to be negatively charged in the active complex, this may be enough to bias NAD^+ toward the hydride transfer conformation. In contrast, a hydrophobic nicotinamide ring would not interact favorably with a charged or polar Cys302, but would form a favorable ring stacking interaction with Phe401 in the hydrolysis position. Solvent accessible area analysis using the CCP4 program areaimol (*21*) with a probe radius of 1.4 Å shows that the nicotinamide ring buries an additional ~5.5 $Å^2$ of hydrophobic surface in the hydrolysis position than in the hydride transfer position. Furthermore, in this position, the nicotinamide ring is capped by the nicotinamide ribose and is less accessible to solvent than in the hydride transfer position. Whether these differences alone are sufficient to favor different binding modes and thus explain the observations from our structures remains to be determined.

It remains plausible that NAD^+ occupies both conformations with equal affinity, and it is the NADH preference for hydrolysis that allows the reaction to proceed. The apparent conformational selectivity observed in the Ser302 mutant could be explained in terms of the replacement of a carbon−sulfur bond with the shorter carbon−oxygen bond, and thereby artificial stabilization of the hydride transfer position for NAD^+, with little effect on NADH binding. However, we believe that our data combined with the data in the literature are best explained by a preference of NADH for the hydrolysis and NAD^+ for the hydride transfer conformation.

ACKNOWLEDGMENT

Use of the Advanced Photon Source at Argonne National Laboratory was supported by the U.S. Department of Energy, Basic Energy Sciences, Office of Science, under Contract W-31-109-Eng-38. Use of the National Synchrotron Light Source at Brookhaven National Laboratory is supported by the U.S. Department of Energy, Division of Materials Sciences and Division of Chemical Sciences, under Contract DE-AC02-98CH10886. We thank the beamline staff at X12B and X12C (NSLS) and at 19ID (APS) for technical assistance.

SUPPORTING INFORMATION AVAILABLE

Data collection, refinement statistics, and temperature factor distributions for the noncovalent complex and the low-magnesium structures (1o01, 1nzx, and 1nzz) (Tables S1 and S2) and omit maps centered on Cys302 for the noncovalent complex (Figure S1). These structures were determined and refined using the same approach discussed in Results. This material is available free of charge via the Internet at http://pubs.acs.org.

REFERENCES

1. Steinmetz, C. G., Peiguang, X., Weiner, H., and Hurley, T. D. (1997) Structure of mitochondrial aldehyde dehydrogenase: The genetic component of ethanol aversion, *Structure 5*, 701−711.
2. Moore, S. A., Baker, H. M., Blythe, T. J., Kitson, K. E., Kitson, T. M., and Baker, E. N., (1998) Sheep liver cytosolic aldehyde dehydrogenase: The structure reveals the basis for the retinal specificity of class 1 aldehyde dehydrogenases, *Structure 6*, 1541−1551.
3. Lamb, A. L., and Newcomer, M. E. (1999) The structure of retinal dehydrogenase type II at 2.7 Å resolution: Implications for retinal specificity, *Biochemistry 38*, 6003−6011.
4. Cobessi, D., Tête-Favier, F., Marchal, S., Azza, S., Branlant, G., and Aubry, A. (1999) Apo and holo crystal structures of an NADP-dependent aldehyde dehydrogenase from *Streptococcus mutans*, *J. Mol. Biol. 290*, 161−173.

5. Johansson, K., El-Ahmad, M., Ramaswamy, S., Hjelmqvist, L., Jörnvall, H., and Eklund, H. (1998) Structure of betaine aldehyde dehydrogenase at 2.1 Å resolution, *Protein Sci. 7*, 2106−2117.
6. Ahvazi, B., Coulombe, R., Delarge, M., Vedadi, M., Zhang, L., Meighen, E., and Vrielink, A. (2000) Crystal structure of the $NADP^+$-dependent aldehyde dehydrogenase from *Vibrio harveyi*: Structural implications for cofactor specificity and affinity, *Biochem. J. 349*, 853−861.
7. Ni, L., Zhou, J., Hurley, T. D., and Weiner, H. (1999) Human liver mitochondrial aldehyde dehydrogenase: Three-dimensional structure and the restoration of solubility and activity of chimeric forms, *Protein Sci. 8*, 2784−2790.
8. Hurley, T. D., Perez-Miller, S., and Breen, H. (2001) Order and disorder in mitochondrial aldehyde dehydrogenase, *Chem.-Biol. Interact. 130*−*132*, 3−14.
9. Hammen, P. K., Allali-Hassani, A., Hallenga, K., Hurley, T. D., and Weiner, H. (2002) Multiple conformations of NAD and NADH when bound to human cytosolic and mitochondrial aldehyde dehydrogenase, *Biochemistry 41*, 7156−7168.
10. Sheikh, S., Ni, L., Hurley, T. D., and Weiner, H. (1997) The potential roles of the conserved amino acids in human liver mitochondrial aldehyde dehydrogenase, *J. Biol. Chem. 272*, 18817−18822.
11. Farrés, J., Wang, T. T. Y., Cunningham, S. J., and Weiner, H. (1995) Investigation of the active site cysteine residue of rat liver mitochondrial aldehyde dehydrogenase by site-directed mutagenesis, *Biochemistry 34*, 2592−2598.
12. Harper, J. K., Lindahl, R., Baker, D. C., and Timkovich, R. (1987) Hydride transfer stereospecificity of rat liver aldehyde dehydrogenases, *J. Biol. Chem. 262*, 10911−10913.
13. Wang, X., and Weiner, H. (1995) Involvement of glutamate 268 in the active site of human liver mitochondrial aldehyde dehydrogenase as probed by site-directed mutagenesis, *Biochemistry 34*, 237−243.
14. Ni, L., Sheikh, S., and Weiner, H. (1997) Involvement of glutamate 399 and lysine 192 in the mechanism of human liver mitochondrial aldehyde dehydrogenase, *J. Biol. Chem. 272*, 18823−18826.
15. Vallari, R. C., and Pietruszko, R. (1984) Interaction of Mg^{2+} with human liver aldehyde dehydrogenase. I. Species difference in the mitochondrial enzyme, *J. Biol. Chem. 259*, 4922−4926.
16. Vallari, R. C., and Pietruszko, R. (1984) Interaction of Mg^{2+} with human liver aldehyde dehydrogenase. II. Mechanism and site of interaction, *J. Biol. Chem. 259*, 4927−4933.
17. Tabor, S., and Richardson, C. C. (1985) A bacteriophage T7 RNA polymerase/promotor system for controlled exclusive expression of specific genes, *Proc. Natl. Acad. Sci. U.S.A. 82*, 1074−1078.
18. Zheng, C. F., Wang, T. T. Y., and Weiner, H. (1993) Cloning and expression of the full-length cDNAS encoding human liver class 1 and class 2 aldehyde dehydrogenase, *Alcohol.: Clin. Exp. Res. 17*, 828−831.
19. Jeng, J. J., and Weiner, H. (1991) Purification and characterization of catalytically active precursor of rat liver mitochondrial aldehyde dehydrogenase expressed in *Escherichia coli*, *Arch. Biochem. Biophys. 289*, 214−222.
20. Ghenbot, G., and Weiner, H. (1992) Purification of liver aldehyde dehydrogenase by p-hydroxyacetophenone-sepharose affinity matrix and the coelution of chloramphenicol acetyl transferase from the same matrix with recombinantly expressed aldehyde dehydrogenase, *Protein Expression Purif. 3*, 470−478.
21. Otwinowski, Z., and Minor, W. (1997) Processing of X-ray diffraction data collected in oscillation mode, *Methods Enzymol. 276*, 307−326.
22. Collaborative Computational Project, Number 4 (1994) The CCP4 suite: Programs for protein crystallography, *Acta Crystallogr. D50*, 760−763.
23. Brünger, A. T., Adams, P. D., Clore, G. M., DeLano, W. L., Gros, P., Grosse-Kunstleve, R. W., Jiang, J.-S., Kuszewski, J., Nilges, N., Pannu, N. S., Read, R. J., Rice, L. M., Simonson, T., and Warren, G. L. (1998) *Crystallography and NMR System*: A new software system for macromolecular structure determination, *Acta Crystallogr. D54*, 905−921.
24. Jones, T. A., Zou, J. Y., Cowan, S. W., and Kjeldgaard, M. (1998) Improved methods for building protein models in electron density maps and the location of errors in these models, *Acta Crystallogr. A47*, 110−119.
25. Guex, N., and Peitsch, M. C. (1997) SWISS-MODEL and the Swiss-PdbViewer: An environment for comparative protein modeling, *Electrophoresis 18*, 2714−2733.
26. Cason, C. J. (1999) *POV-Ray for Windows*, version 3.1, http://www.povray.org/.
27. Murchudov, G. N., Vagin, A. A., and Dodson, E. J. (1997) Refinement of macromolecular structures by the maximum-likelihood method, *Acta Crystallogr. D53*, 240−225.
28. Nayal, M., and Di Cera, E. (1996) Valence screening of water in protein crystals reveals potential Na^+ binding sites, *J. Mol. Biol. 256*, 228−234.
29. Rossmann, M. G., Moras, D., and Olsen, K. W. (1974) Chemical and biological evolution of a nucleotide-binding protein, *Nature 250*, 194−199.
30. Carugo, O., and Argos, P. (1997) NADP-dependent enzymes. I: Conserved stereochemistry of cofactor binding, *Proteins: Struct., Funct., Genet. 28*, 10−28.
31. Carugo, O., and Argos, P. (1997) NADP-dependent enzymes. II: Evolution of the mono- and dinucleotide binding domains, *Proteins: Struct., Funct., Genet. 28*, 29−40.
32. Eklund, H., Samama, J.-P., and Jones, T. A. (1984) Crystallographic investigations of nicotinamide adenine dinucleotide binding to horse liver alcohol dehydrogenase, *Biochemistry 23*, 5982−5996.
33. Niederhut, M. S., Gibbons, B. J., Perez-Miller, S., and Hurley, T. D. (2001) Three-dimensional structures of the three human class 1 alcohol dehydrogenases, *Protein Sci. 10*, 697−706.
34. Colonna-Cesari, F., Perahia, D., Karplus, M., Eklund, H., Brändén, C. I., and Tapia, O. (1986) Interdomain motion in liver alcohol dehydrogenase, *J. Biol. Chem. 261*, 15273−15280.
35. Vallari, R. C., and Pietruszko, R. (1981) Kinetic mechanism of the human cytoplasmic aldehyde dehydrogenase E1, *Arch. Biochem. Biophys. 212*, 9−19.
36. Dryjanski, M., Lehmann, T., Abriola, D., and Pietruszko, R. (1999) Binding and incorporation of 4-*trans*-(*N*,*N*-dimethylamino)cinnamaldehyde by aldehyde dehydrogenase, *J. Protein Chem. 18*, 627−636.
37. Rout, U. K., and Weiner, H. (1994) Involvement of serine 74 in the enyzme-coenzyme interaction of rat liver mitochondrial aldehyde dehydrogenase, *Biochemistry 33*, 8955−8961.

BI034182W